Atmos. Meas. Tech. Discuss., https://doi.org/10.5194/amt-2019-46
Manuscript under review for journal Atmos. Meas. Tech.
Discussion started: 18 March 2019

Atmospheric Measurement Techniques Discussions

Validation, comparison, and integration of GOCI, AHI, MODIS, MISR, and VIIRS aerosol optical depth over East Asia during the 2016 KORUS-AQ campaign

Myungje Choi[1,2], Hyunkwang Lim[2], Jhoon Kim[2], Seoyoung Lee[2], Thomas F. Eck[3, 4], Brent N. Holben[4], Michael J. Garay[1], Edward J. Hyer[5], Pablo E. Saide[6]

[1]Jet Propulsion Laboratory, California Institute of Technology, Pasadena, California, USA
[2]Department of Atmospheric Sciences, Yonsei University, Seoul, Republic of Korea
[3]Universities Space Research Association, Columbia, MD, USA
[4]NASA Goddard Space Flight Center, Greenbelt, MD, USA
[5]Marine Meteorology Division, Naval Research Laboratory, Monterey, CA, USA
[6]Department of Atmospheric and Oceanic Sciences, Institute of the Environment and Sustainability, University of California–Los Angeles, Los Angeles, CA, USA

Correspondence to: Jhoon Kim (jkim2@yonsei.ac.kr); Myungje Choi (myungje.choi@jpl.nasa.gov)

Abstract

Recently launched multi-channel geostationary-Earth-orbit (GEO) satellite sensors such as the Geostationary Ocean Color Imager (GOCI) and the Advanced Himawari Imager (AHI) provide aerosol products over East Asia with high accuracy, which enables the monitoring of rapid diurnal variations and the transboundary transport of aerosols. Most aerosol studies to date have used low-Earth-orbit (LEO) satellite sensors, such as the Moderate Resolution Imaging Spectroradiometer (MODIS) and the Multi-angle Imaging SpectroRadiometer (MISR) with a maximum of one or two overpass daylight times per day at mid- to low latitudes. Thus, the demand for new GEO observations with high temporal resolution and improved accuracy has been significant. In this study the aerosol optical depth (AOD) products from three LEO sensors—MODIS, MISR, and the Visible/Infrared Imager Radiometer Suite (VIIRS)—along with two GEO sensors—GOCI and AHI—are validated, compared and integrated for the period during the Korea–United Sates Air Quality Study (KORUS-AQ) field campaign from 1 May to 12 June 2016 over East Asia. The AOD products analyzed here generally have high accuracy, but their error characteristics differ according to the use of several different surface-reflectance estimation methods plus differences in cloud screening. High-accuracy near-real-time GOCI and AHI measurements facilitate the detection of rapid AOD changes, such as smoke aerosol transport from Russia to Japan on 18–21 May 2016, heavy pollution transport from China to Korea on 25 May 2016, and local emission transport from the Seoul Metropolitan Area to the Yellow Sea in Korea on 5 June 2016. These high-temporal-resolution GEO measurements result in more-representative daily AOD values and make a greater contribution to a combined daily AOD product assembled by median-value selection with a 0.5° × 0.5° grid resolution. The combined AOD is more spatially continuous and of higher accuracy than the individual products. This study characterizes aerosol measurements

Atmos. Meas. Tech. Discuss., https://doi.org/10.5194/amt-2019-46
Manuscript under review for journal Atmos. Meas. Tech.
Discussion started: 18 March 2019

Atmospheric Measurement Techniques Discussions

from LEO and GEO satellites currently in operation over East Asia, and results presented here can be used to evaluate satellite measurement bias and air-quality models.

1 Introduction

Atmospheric aerosol particles are composed of solid and liquid matter and have diameters of a few nanometers up to several micrometers and lifetimes of one to tens of days. Aerosol particles affect the atmospheric radiation balance by scattering and absorbing incident top-of-atmosphere (TOA) sunlight and that scattered from the surface, as well as by interacting with clouds (e.g., by changing cloud distributions, optical properties, and precipitation by acting as cloud condensation nuclei) with global climate effects (IPCC, 2013). Global net radiative cooling or heating is determined partially by interactions for which the level of understanding is still low and varies significantly with geographic region. Additionally, ambient particulate matter (PM) at the ground level adversely affects human health through pulmonary and respiratory transport, resulting in heart disease, stroke, and lung cancer (Lim et al., 2012). Many developing countries in East Asia have both large anthropogenic emission sources and natural aerosol sources, such as the Taklamakan and Gobi deserts and wild-fire regions. For this reason, East Asia currently has one of the most heavily polluted atmospheres in the world (Kim et al., 2007; Yoon et al., 2014).

Aerosol measurements are routinely conducted at diverse scales by laboratory experiments, in situ measurements and remote sensing, and from various platforms including ground-based, airborne, ship-borne, and satellite sensors. Accurate microphysical and chemical properties of aerosols can be obtained from laboratory experiments or ground-based/airborne measurements, but their spatial coverage is limited. Satellite-based remote sensing measurements provide aerosol optical properties, including aerosol optical depth (AOD), over much broader areas. Currently operating low-Earth-orbit (LEO) satellite sensors such as the Moderate Resolution Imaging Spectroradiometer (MODIS), the Multi-angle Imaging SpectroRadiometer (MISR), and the Visible/Infrared Imager Radiometer Suite (VIIRS) provide global aerosol information, but at a temporal resolution that is limited to once per day at least, but typically once every 2–3 days due to cloud cover. Most satellite-based aerosol retrieval techniques and algorithms have been developed for these LEO sensors (Kaufman et al., 1997; Diner et al., 1998; Torres et al., 1998; Higurashi and Nakajima, 1999; Hsu et al., 2004; Remer et al., 2005). To overcome temporal resolution limitation, there were several attempts to retrieve AOD using first-generation meteorological geostationary satellites such as the Geostationary Operational Environmental Satellite (GOES), the Geostationary Meteorological Satellite (GMS), and the Multifunction Transport Satellite (MTSAT), but they showed worse accuracy than those of LEO sensors due to the wider and fewer visible channels with coarser spatial resolution which make difficult to distinguish aerosol types (Knapp et al., 2002; Wang et al., 2003; Urm and Sohn, 2005; Kim et al., 2008; Yoon et al., 2007). As the specifications of recently launched geostationary-Earth-orbit (GEO) sensors such as the Geostationary Ocean Color Imager (GOCI) and the Advanced Himawari Imager (AHI) over East Asia and the Advanced Baseline Imager (ABI) over the United States are approaching those of current LEO sensors, aerosol optical properties can be retrieved with accuracy as high as that of LEO sensors, and at much higher temporal resolutions, from a few minutes to one hour during daylight hours (Lim et al., 2018; Choi et al., 2018; Lee et

al., 2010; Choi et al., 2016; Kikuchi et al., 2018; Zhang et al., 2018; Daisaku, 2016; Chen et al., 2018; Laszlo and Liu, 2016). This breakthrough in temporal resolution of GEO aerosol data enables us to monitor highly variable aerosol conditions and improve air-quality forecasting, particularly for PM, with data assimilation (Park et al., 2014; Saide et al., 2014; Jeon et al., 2016; Lee et al., 2016; Pang et al., 2018) or machine learning (Park et al., 2018). For these reasons, the demand for GEO aerosol measurements is high.

Some satellite aerosol retrieval algorithms have been improved toward higher spatial resolution (e.g. 5-10 km or finer), higher temporal resolution (e.g. from daily to hourly and few minutes resolution), vertical distribution information, and high accuracy of other optical properties such as particle size or absorptivity beyond high accuracy of AOD to obtain more accurate ground level $PM_{2.5}$ concentration and its species (Diner et al., 2018) and also to fulfill the requirement for understanding of long-term climatological changes (GCOS, 2016).

Several field campaigns have been performed over East Asia to investigate aerosol chemical, microphysical, and optical properties based on in situ and remote-sensing measurements. These include the Transport and Chemical Evolution over the Pacific (TRACE-P) aircraft campaign in 2001 (Jacob et al., 2003), the Atmospheric Brown Cloud–East Asia Regional Experiment (ABC–EARES) in 2005 (Nakajima et al., 2007), the Distributed Regional Aerosol Gridded Observation Networks (DRAGON)–Asia campaign in 2012 (Holben et al., 2018), and the Megacity Air Pollution Studies (MAPS) in 2015 (Kim et al., 2018). Aerosol retrieval algorithms have been developed, improved, and validated using the extensive measurement datasets obtained from these field campaign studies (Kim et al., 2016; Jeong et al., 2016; Kim et al., 2007; Lee et al., 2018; Xiao et al., 2016; Garay et al., 2017).

The Korea–United Sates Air Quality Study (KORUS-AQ; https://www-air.larc.nasa.gov/missions/korus-aq/) was performed over Korea from 1 May to 12 June 2016 under the leadership of Korea's National Institute of Environmental Research (NIER) and the United States National Aeronautics and Space Administration (NASA). One of the main objectives of the campaign was to evaluate and improve satellite aerosol retrieval algorithms using in situ and remote-sensing measurements (Goto et al., 2019; Lennartson et al., 2018). These efforts, based on comparisons of satellite aerosol products, will eventually lead to improved air quality models. During the campaign, GOCI aerosol optical properties were retrieved and provided to support air-quality forecasting, determination of the flight plan for aircraft measurements to detect heavy pollution plumes, and data assimilation using near-real-time chemical transport model simulations (Saide et al., 2014; Choi et al., 2018). Here, in addition to the GOCI AOD dataset, the latest versions of AOD datasets from LEO sensors (MODIS, MISR, and VIIRS) and another GEO sensor (AHI) are validated, compared, and integrated for the period of the field campaign. The latest version of the Aerosol Robotic Network (AERONET) of ground-based sun photometers dataset (Version 3) over East Asia is used as a reference for the campaign period (Eck et al., 2018; Giles et al., 2019). Characteristics of the various AOD products are analyzed for specific transport cases with high temporal resolution at the daily scale over the campaign period.

The remainder of this paper is organized as follows. In Sect. 2, satellite and ground-based remote sensing data used in this study are summarized. In Sect. 3, the various AOD products are validated and compared using ground-based AERONET observations separately over ocean and land. The specific aerosol loading cases during the campaign are analyzed in Sect. 4.

In Sect. 5, daily representative AOD is generated on a common spatial grid for each product and used to calculate the mean AOD distribution during the campaign. The daily AOD integration is tested using multiple AOD products at the daily scale. Finally, a discussion and conclusions are presented in Sect. 6.

2 Satellite and ground-based AERONET aerosol data

2.1 GOCI Yonsei aerosol product

The GOCI is a unique ocean color sensor in GEO (longitude 128.2°E) on board of the Korean Communication, Ocean, and Meteorological Satellite (COMS) and has been making observations over East Asia since 2010. It covers a 2500 km × 2500 km area centered over the Korean Peninsula, such that the eastern part of China and Japan are also covered at a 500 m × 500 m spatial resolution and 1 h temporal resolution from 09:30 to 16:30 local time (total of 8 measurements during daylight hours). Aerosol optical depth at 550 nm is retrieved using the GOCI Yonsei aerosol retrieval (YAER) algorithm at a 6 km × 6 km spatial resolution after masking pixels affected by clouds or sun-glint and aggregating the remaining pixels to provide aerosol signals at the resolution of the reflectance measurements. Land-surface reflectance is obtained using the minimum reflectance technique for each month and hour of Rayleigh-corrected reflectance measurements (Hsu et al., 2004; Herman and Celarier, 1997; Koelemeijer et al., 2003). Ocean-surface reflectance is based on the Cox–Munk ocean bidirectional reflectance distribution function (BRDF) (Cox and Munk, 1954). Details of the aerosol retrieval algorithm, and the improvement and validation results for March 2011 to February 2017, are presented by Choi et al. (2016). According to Choi et al. (2018), the GOCI YAER version 2 AOD has a positive bias that increases with the geometrical cloud fraction, particularly near cloud edges, and the remaining cloud contamination was largely due to the absence of infrared (IR) measurement in GOCI. Thus, in this study, additional cloud masking is applied to the GOCI cloud-masking procedure, using Himawari-8 IR data. Details of the AHI IR cloud-masking procedure for aerosol retrieval are described by Lim et al. (2018).

2.2 AHI Yonsei aerosol product

The AHI, onboard the Himawari-8 and -9 satellites, is part of a new generation of meteorological satellite sensors. Compared with previous meteorological sensors, such as the Japanese Advanced Meteorological Imager (JAMI) onboard the Japanese Multifunction Transport Satellite–1R (MTSAT–1R; also referred to as Himawari-6) or the Meteorological Imager (MI) onboard the Korean COMS satellite, the AHI has more channels (16) including 3 visible channels (0.47, 0.51, and 0.64 μm) with higher spatial resolution (0.5 to 2.0 km). The addition of more visible channels to the one broad visible channel of JAMI and MI enables aerosol type classification and improves aerosol retrieval accuracy. However, the primary advantage of AHI is the high temporal resolution: 2.5 min over Japan and 10 min over the full-disk area centered at 140.7°E. The full-disk observation area covers East Asia (eastern India, Southeast Asia, Korea, Japan, most of China, and parts of Russia and Oceania). The AHI Yonsei aerosol retrieval algorithm applies two distinct schemes (Lim et al., 2018). The first scheme is based on the Dark-Target approach over land using a 1.6 μm short-wave infrared (SWIR) channel and the Cox–Munk ocean

BRDF model with chlorophyll-*a* to simulate the water-leaving radiance over the ocean, referred to as the Estimated Surface Reflectance (ESR) method. Official AHI JAXA chlorophyll-*a* concentration data are spatiotemporally interpolated to the AHI Yonsei aerosol product pixels and used to calculate the ocean-surface reflectance. The second scheme is based on the minimum surface reflectance over land and ocean, referred to as the Minimum Reflectance Method (MRM). The AHI YAER algorithm provides two versions of 550 nm AOD with a 6 km × 6 km spatial resolution. Details of the AHI YAER algorithm are presented by Lim et al. (2018). The full-disk area is measured by AHI in ten segments from north to south. The 2nd and 3rd segments approximately cover the area 20°N–48°N and are used to retrieve AOD using the YAER algorithm in this study.

2.3 MODIS Dark-Target aerosol product

The MODIS is one of the most widely used instruments for global aerosol measurements. It has been in operation onboard the NASA Terra (10:30 descending) satellite since 1999 and the Aqua (13:30 ascending) satellite since 2002. In general, MODIS measurements employ single-angle viewing, multiple channels (36 channels), high spatial resolution (0.25 to 1.00 km according to channel), and a wide swath (2330 km) enabling daily global coverage for short-wave channels. The MODIS Dark-Target (DT) aerosol retrieval algorithm uses the broader-bandwidth MODIS channels (>20 nm) in the visible to SWIR range. The DT algorithm assumes that land-surface reflectance in the visible range has a linear relationship with SWIR (2.1 μm) surface reflectance, where the atmospheric signal is low (Kaufman et al., 1997), that varies according to the Normalized Difference Vegetation Index (NDVI). This approach is applied to dark land surfaces; e.g., vegetated areas. Ocean-surface reflectance is based on Fresnel reflectance with the Cox–Munk assumption. The MODIS DT algorithm uses NCEP wind-speed analysis data as input and calculates ocean-surface reflectance according to geometry and wind speed. The MODIS DT AOD at 550 nm is provided at 10 km × 10 km and 3 km × 3 km spatial resolution at nadir after pixel aggregation at the spatial resolution of the reflectance data. In this study, the latest version "Collection 6.1 (C6.1)" data of only the best quality ("Quality Assurance Flag 3") land and ocean 550 nm AOD for both resolutions are used (Levy et al., 2013; Munchak et al., 2013; Gupta et al., 2016).

2.4 MODIS Deep-Blue aerosol product

The MODIS Deep-Blue (DB) aerosol product uses ocean color channels and IR channels to retrieve aerosol optical properties over bright land surfaces. Using the enhanced DB algorithm, MODIS DB AOD is retrieved over arid/semi-arid surfaces, natural vegetation areas, and urban, built-up, and transitional regions using several surface-reflectance calculations. These calculations use a pre-calculated surface reflectance database with the minimum reflectance technique, a DT-like approach, and a hybrid method over arid/semi-arid surfaces, vegetation, and urban, built-up, and transition surfaces. The MODIS DB algorithm calculates AOD for each of the original L1B 1 km pixels, and aggregates and averages retrieved AOD pixels to 10 km × 10 km resolution at nadir after appropriate masking procedures that differ from those in the MODIS DT and GOCI

YAER algorithms. The latest version C6.1 MODIS DB land 550 nm AOD of only the best quality is also used in this study (Hsu et al., 2013; Sayer et al., 2013).

2.5 VIIRS EDR aerosol product

The VIIRS is a sensor onboard the Suomi-NPP satellite, which was launched in October 2011. The general characteristics of VIIRS are similar to those of MODIS, and include single-angle viewing, multiple channels (22 channels), high spatial resolution (375–750 m), and a wide swath (3,040 km) that results in no gaps between adjacent swaths near the equator. The VIIRS aerosol Interface Data Processing Segment (IDPS) products provided by NOAA consist of two products: the Environmental Data Record (EDR) and the Intermediate Product (IP). The VIIRS aerosol retrieval algorithm is similar to the Dark-Target algorithm in terms of the coupling of land-surface reflectance in the visible range using the SWIR channel (2.25 μm), ocean-surface reflectance that considers wind speed and direction using the Cox–Munk model with Fresnel reflectance, and a combination of fine- and coarse-aerosol models. However, the channel selection and threshold values for each procedure in the algorithm differ from those of MODIS. Details of the VIIRS aerosol retrieval algorithm, including similarities and differences with the MODIS aerosol retrieval algorithm, are described by Jackson et al. (2013) and Huang et al. (2016). The IP aerosol product is calculated at a 0.75 km × 0.75 km spatial resolution at nadir, and the EDR product is generated by aggregating 8 × 8 IP pixels (6 km × 6 km at nadir) after additional masking. In this study, the VIIRS EDR 550 nm AOD is used.

2.6 MISR aerosol product

The MISR is one of the sensors onboard the Terra satellite along with MODIS. Unique characteristics of MISR include multi-channel (four wavelengths, centered at 446, 558, 672, and 866 nm) and multi-angle measurements (nine cameras; nadir, ±26.1°, ±45.6°, ±60.0°, and ±70.5°), which enable better detection of aerosol particle shapes and a distinction between atmospheric and surface signals through calculation of surface bidirectional reflectance factors (BRF). The MISR spatial resolutions at nadir and off-nadir are 250 m × 250 m and 275 m × 275 m, respectively, and the operational MISR aerosol retrieval algorithm provides 550 nm AOD and other optical properties at 17.6 km × 17.6 km in version 22 and 4.4 km × 4.4 km in version 23 after pixel masking and aggregation at the spatial resolution of the reflectance data. Targeted surface conditions for aerosol retrieval are dark ocean, dark vegetation, and bright arid land surfaces. One advantage of MISR measurements is the absence of non-retrieval areas caused by sun-glint effects that are present in nadir-only viewing measurements, such as MODIS. The swath is ~380 km, which is narrower than MODIS, and results in global coverage every 9 days with repeat coverage between 2 and 9 days depending on latitude (2–3 days near the Korean Peninsula). In this study, version 23 AOD at 550 nm is used (Garay et al., 2017; Witek et al., 2018).

2.7 AERONET measurements during the KORUS-AQ campaign

To evaluate the various satellite AOD products during the 2016 KORUS-AQ campaign (1 May to 12 June 2016), extensive data from ground-based remote-sensing AERONET sun photometers were collected from total 33 sites over East Asia including 19 Korean sites (Holben et al., 2018; Holben et al., 1998). Detailed site information, including locations, is available at the AERONET homepage (https://aeronet.gsfc.nasa.gov/new_web/DRAGON-KORUS-AQ_2016.html). AERONET provides high accuracy measurement of AOD with uncertainty of ~0.01 in the mid-visible (Eck et al., 1999). The AERONET Version 3 Level 2.0 AOD at 550 nm all-points data at a few-minutes temporal resolution are used (Holben et al., 2018; Eck et al., 2018). To compare satellite and ground-based AERONET AOD, spatiotemporal collocation is implemented. This study follows the general collocation criteria of Sayer et al. (2014): satellite pixels within a 25 km radius of each AERONET site are spatially averaged, and AERONET data within a ±30 min window around the satellite measurements are temporally averaged. Note that the 10 min interval AHI AOD data are collocated with AERONET AOD within a ±5 min temporal window. Because there are only a few AERONET sites surrounded by ocean, AERONET sites located on a coast are used to validate satellite ocean AOD. Also note that a collocated sample is included in the average if at least one measurement is available.

3 Validation results

3.1 Statistical metrics

The statistical metrics as used by Sayer et al. (2014) were also applied here for comparison of satellite AOD measurements over land and ocean and are summarized in Tables 2 and 3, respectively. Because the distribution of AOD is non-Gaussian and skewed towards low values, AOD evaluation is difficult using simple statistical techniques. Thus, the metrics applied here consist of the number of matched/collocated data points (N), Pearson's linear correlation coefficient (R), the root mean square error ($RMSE$), the mean bias (MB) error, and the fraction within the expected error of MODIS Collection 5 DT land AOD [f within EE_{DT}, or f where $EE_{DT} = \pm (0.05 + 0.15 \times \text{AERONET AOD})$], as suggested by Levy et al. (2007).

3.2 Land AOD validation

Each satellite measures the area within its swath at different times during daylight hours, as listed in Table 1. In contrast to the hourly and 10 min interval measurements of GOCI and AHI, respectively, the LEO satellites observe East Asia only once per day. The overpass time for Terra is at 10:30 Local Standard Time [LST; Coordinated Universal Time (UTC) + 9] and those for Aqua and Suomi-NPP are at 13:30 LST and 13:25 LST, respectively. When measurement times are similar, N can be determined by swath, spatial resolution, and the quality assurance flag, among other factors. Because of gaps arising from its narrow swath, MISR does not fully cover East Asia in one day. This results in the lowest N (114) for land AOD. In contrast, the other sensors have wider swaths that cover most of East Asia in one day, resulting in higher N (413–661) over land. The

Atmos. Meas. Tech. Discuss., https://doi.org/10.5194/amt-2019-46
Manuscript under review for journal Atmos. Meas. Tech.
Discussion started: 18 March 2019

Atmospheric Measurement Techniques Discussions

MISR land AOD has the highest *f* within EE_{DT} (81%) and lowest *MB* (−0.02) compared with other land AODs (*f* of 43%–59% and absolute value of *MB* > 0.06).

For the lowest-valued land AOD bin in Fig. 1a, the GOCI and AHI MRM AOD are negatively biased and the AHI ESR and MODIS DT AOD are positively biased. The GOCI and AHI MRM aerosol retrieval algorithms obtain surface reflectance using the minimum reflectivity technique with monthly samples of Rayleigh-corrected reflectance (RCR). Although this technique is designed to obtain cloud-free and aerosol-free conditions by finding dark pixels within the composite dataset, the calculations can still be affected by aerosols and clouds, resulting in overestimated surface reflectance. The climatological surface-reflectance database of GOCI did not show negatively biased AOD between 2011 and 2014, but starts to show a negative bias in 2015, according to the validation study of Choi et al. (2018). This recent negative bias in 2015 and 2016 may be due to a sensor calibration issue or degradation, but the exact cause is difficult to diagnose and remains unknown.

The AHI ESR and MODIS DT (both 10 km and 3 km products) AOD is positively biased under low-AOD conditions. Both algorithms assume a surface reflectance based on an empirical linear relationship between the visible and SWIR channels. Some studies indicate that MODIS Collection 6 DT AOD does not have a noticeable positive *MB* (Levy et al., 2013; Sayer et al., 2014) globally or over East Asia, but other studies have reported a positive bias in MODIS C6 DT AOD over East Asia (Choi et al., 2018; Xiao et al., 2016), particularly over urban areas. Although the algorithm was modified to improve AOD accuracy over urban areas starting with Collection 6.1, MODIS DT still overestimates AOD compared with AERONET over East Asia (Gupta et al., 2016). In addition, the DT algorithm is designed for global retrievals and is not optimized for East Asia, which may explain the observed bias. The VIIRS algorithm is similar to the MODIS DT algorithm, and is also positively biased. The MODIS DB AOD and MISR AOD are less biased in the low-AOD range compared with the other sensors, which is consistent with previous studies (Choi et al., 2018; Garay et al., 2017; Sayer et al., 2014).

3.3 Ocean AOD validation

The target area for ocean aerosol retrievals differs among the various algorithms. The MODIS DT, MISR, and VIIRS algorithms retrieve aerosol properties only for dark-ocean pixels, which means that surface pixels that are not completely dark, such as those containing shallow or turbid water, are masked. The GOCI and AHI Yonsei aerosol algorithms are also designed to retrieve aerosols over dark pixels, but they include moderately turbid water pixels by considering the climatological ocean-surface reflectance based on minimum-reflectance techniques in the GOCI and AHI MRM algorithms and by considering chlorophyll-*a* concentrations in the AHI ESR algorithm. Because the ocean AOD validation was conducted using coastal AERONET AOD observations, *N* is higher for GOCI and AHI (230–237) than for the LEO ocean AOD observations (13–111), with the exception of the VIIRS ocean AOD (252). Sun-glint areas also likely contribute to the difference in *N*. Single-angle viewing LEO satellite measurements, such as MODIS, exclude bright ocean-surface pixels because of sun-glint close to nadir, where most pixels are screened out, as is evident in Fig. 2. This occurs daily near the Korean Peninsula and results in most transported aerosol plumes around Korea not being measured with continuous spatial coverage. Although the VIIRS is also a single-angle viewing instrument, its broader swath results in more ocean pixels being retrieved than is the case for

MODIS. The MISR instrument minimizes sun-glint effects over ocean pixels through multi-angle viewing, but still has low *N* because of its narrow swath. The sun-glint areas of the GEO satellites are located near the equator, have a circular shape, and shift from east at sunrise to west at sunset. Most SE Asian countries, including the Philippines, Malaysia, and Thailand, are affected by this sun-glint screening in ocean AOD from GEO satellites, whereas most northeast (NE) Asian countries, including China, Korea, and Japan, are unaffected. Thus, GOCI and AHI provide spatiotemporally continuous aerosol measurements across land and ocean over NE Asia where dense aerosol plumes of varying composition are transported from mainland Asia to the Pacific.

According to most validation metrics, ocean AOD products are more accurate than those over land. This difference leads to generally lower errors for ocean AOD compared to their respective over land retrievals, based on AERONET AOD measurements (Fig. 1b). The sign of the ocean AOD error in the low-AOD range is the same as that of the land AOD error for all products; i.e., negative in GOCI and AHI MRM, and positive in DT and AHI ESR. The VIIRS, GOCI, and AHI products have high accuracy, as evidenced by a low RMSE (0.117–0.128) and a near-zero *MB* (−0.034 to 0.037), resulting in a high *f* (0.612–0.769). For MODIS DT ocean AOD, measurements from the Aqua satellite are more accurate than those from the Terra satellite, which can be attributed to their individual calibrations (Levy et al., 2018). The 3 km ocean AOD product has a larger positive *MB* (0.098) than the 10 km product (0.064), as is the case for MODIS DT land AOD (0.113 and 0.150 for 10 km and 3 km, respectively).

In summary, the various LEO and GEO aerosol products over East Asia are highly accurate based on a comparison with AERONET, but have unique bias patterns related to the surface-reflectance assumptions in each algorithm. This leads to positive biases for MODIS DT and AHI ESR AOD, negative biases for GOCI and AHI MRM AOD, and small biases for the other products. The coverage also differs between single-angle and multi-angle measurements, and with swath size and orbit types, resulting in a range of *N* values.

4 Transport events during the campaign

4.1 Analysis of the period 18–21 May 2016 over Hokkaido, Japan

The period 18–21 May 2016 over Hokkaido, Japan included aerosol transport observed during the campaign. Although GOCI and AHI AOD were retrieved at 1 h and 10 min temporal resolutions, respectively, only data for 09:30 and 13:30 LST are presented in Fig. 2 for comparison with Terra, Aqua, and Suomi-NPP AOD distributions. A time series of satellite AOD collocated with AERONET AOD from the Hokkaido University, which is located at 142.34°E longitude, 43.08°N latitude, and 43.08 m altitude above sea level, is presented in Fig. 3.

As the dense smoke aerosol plume (AOD > 2.0 at the center) generated due to the Russian forest fires was transported to Hokkaido continuously from morning to afternoon on 18 May, AERONET AOD at Hokkaido University increased rapidly from 0.1 to 1.4, and the GOCI and AHI successfully detected this sudden increase. The MODIS and VIIRS instruments also detected this plume but the first and last AOD retrievals during the day were 0.6 and 1.1 at 10:30 and 13:30 LST, respectively,

and therefore did not capture the full diurnal variation detected by AERONET, GOCI, and AHI. The increase of AOD at Hokkaido on 18 May was anticipated from the southward movement of the plume revealed by the GOCI and AHI measurements. On 19 May, the plume remained over Hokkaido and the spatial distribution changed little during daylight hours. The AOD observed by AERONET decreased from 1.3 to 0.9, and the GOCI and AHI instruments detected this change, but with a slight overestimation during the morning. The VIIRS AOD shows good agreement with AERONET, but the MODIS DT and DB AODs are higher (~1.5) and the MISR AOD is lower (~0.9) than the AERONET value. On 20 May, the AERONET AOD increased beginning at 06:00 LST (1.0), peaked at 12:00–13:00 LST (1.3), and sharply decreased at 18:00 LST (~0.6). The GOCI and AHI instruments again detected this variation well, beginning at 09:00 LST. The AHI instrument also detected the AOD peak well, but the MODIS DT and DB overestimated AOD compared with AERONET. The pixels involved did not include cloud edges, so this difference in AOD was not due to cloud contamination. The Hokkaido university AERONET site AE between 440 nm and 870 nm was around 1.95 and that of SSA at 440 nm was about 0.9, which means that those aerosols were small particle size and less absorbing as a smoke plume. On 21 May, a central portion of the dense AOD plume dispersed and the plume became elongated in the south–west direction. The AERONET AOD over the Hokkaido University site decreased slightly from 0.6 to 0.4 and most products detected these low-AOD conditions well.

As revealed by a time series analysis and comparison of spatial distributions, the GOCI and AHI AODs have continuous spatiotemporal distributions during daytime with wide coverage around the Hokkaido area and high accuracy compared to the LEO sensors. Additionally, MODIS and VIIRS do not provide spatially continuous AOD distributions because of sun-glint masking over ocean areas near Hokkaido, making identification of plume sources and transport pattern difficult.

4.2 Analysis of 25 May 2016 and 5 June 2016 over the Korean Peninsula

During the campaign, the first noticeable increase in PM above the Korean national air-quality standard (50 μg m^{-3}) occurred on 25 May 2016 and resulted in dense aerosol conditions around the Korean Peninsula. The GOCI AOD distribution from 09:30 to 15:30 LST at a 2 h interval is presented as Fig. 4a–d. High AOD values ranging from 0.8 to 2.0 were measured over the Yellow Sea, located to the west of the Korean Peninsula, at 09:30 LST. A few land pixels in the southwestern Korean Peninsula adjacent to this dense aerosol plume also showed high AOD values of ~1.0. Land pixels in the northwestern Korean Peninsula and adjacent ocean pixels were screened out because of clouds, and other land pixels over the eastern Korean Peninsula had very low AOD values (0.0–0.3). As the plume continuously moved eastward, high AOD conditions entered land pixels in the Korean Peninsula and a steep zonal gradient of AOD was evident near 127°E at 15:30 LST, as shown in Fig. 4d. To evaluate the hourly AOD transportation quantitatively, AOD pixels within the domain shown in Fig. 4 were averaged meridionally at a 0.02° longitude interval as shown in Fig. 5a. The peak at 09:30 LST was located at ~123.5°E and moved continuously eastward to 123.8°E, 124.4°E, 124.8°E, 125.0°E, 125.5°E, 125.8°E, and 126.3°E at 1 h intervals until 16:30 LST. The AOD over the Yellow Sea (123°E–126°E) decreased from 1.2 to 0.9 as the plume was transported. In contrast, the AOD over the Korean Peninsula (126°E–129.5°E) increased gradually, particularly over 127°E

in the western Korean Peninsula where it increased from 0.3 to 0.8. The eastern Korean Peninsula (128°E–129.5°E) was not affected by the plume during daylight hours, and the AOD remained low (0.2–0.3).

Compared with conditions on 25 May 2016, the overall AOD on 5 June 2016 over the Yellow Sea and Korean Peninsula was low (0.1–0.2) and the AOD over the Seoul Metropolitan Area (SMA) near 127°E and 37°N was ~0.3 at 09:30 LST, as shown in Fig. 4e. The focus here is on SMA AOD, which increased up to 0.6 and diffused into surrounding areas in the afternoon, as shown in Fig. 4f–h. Because the periphery of the SMA remained under low-AOD conditions and aerosol transport from China through the Yellow Sea was not detected, this increase can be attributed to local emissions. A distinct pattern is evident in the hourly meridional mean AOD distribution shown in Fig. 5b. The mean AOD in the region 125.5°E–127.0°E gradually increased from 0.2 to 0.5, whereas the AOD in other areas, including the Yellow Sea and eastern Korean Peninsula, remained constant during daylight hours. Unlike conditions on 25 May, the dense aerosol plume on 5 June grew rapidly over a short period of time from local-area emissions and was transported to the Yellow Sea.

The two events analyzed in this section involved rapid changes in hourly AOD, but have noticeably different spatiotemporal characteristics, leading to high-AOD conditions that are attributed to either long-range transboundary transport from China or local emissions in Korea. To accurately assess these types of events, spatiotemporally continuous measurements with minimal data gaps are required, and are currently possible only from GEO measurements.

5 Comparison of spatial distribution and daily AOD integration

5.1 Averaging daily and campaign-period AOD on a common grid

Because the various satellite AOD products were validated using AERONET, results are only valid for specific ground sites. A comparison between satellite products can provide the relative difference in AOD for each pixel, but a direct comparison between satellite products of Level 2 (L2) data is difficult because they differ in spatial coverage, measurement time, and spatiotemporal resolution. For this reason, each L2 AOD product was regenerated as a daily average value on the spatial grid of the Level 3 (L3) products. Although some products are available in the L3 format, the methods and criteria used in their L3 calculation differ considerably. Thus, a simple and commonly used method is applied here to generate daily L3 AOD. The spatial domain is set to 110°E–150°E and 20°N–50°N, and the grid resolution is set to 0.5° × 0.5°. For the aggregation, textural filtering described by Zhang and Reid (2006) and Hyer et al. (2011) is used to reduce random error through averaging. Then, AOD pixels within a grid cell are filtered if the number of retrieved AOD pixels is <3 or the coefficient of variation of AOD within the grid cell is >0.5 and the mean AOD is >0.2. The number of pixels used to calculate one 0.5° × 0.5° pixel is determined by the spatial resolution of the L2 AOD data and the number of filtered pixels. After aggregation of each distribution to the L3 grid, the distributions for each day are averaged to a daily mean value. Temporal resolution and swath determine the maximum number of temporal samples used in the daily mean value: 8 for GOCI (1 h temporal resolution), 47 for AHI (10 min temporal resolution), 2–4 for MODIS (Aqua and Terra), and 1 or 2 (swath-overlapped pixels) for VIIRS and MISR.

Atmos. Meas. Tech. Discuss., https://doi.org/10.5194/amt-2019-46
Manuscript under review for journal Atmos. Meas. Tech.
Discussion started: 18 March 2019

5.2 Comparison of mean AOD distributions during the campaign

The resulting daily gridded AOD products are averaged over the campaign period and presented as Fig. 6a–g. High AOD in eastern China, low AOD in Japan, high AOD in western Korea, and low AOD in eastern Korea are common characteristics of all the products, with the exception of MISR. The narrow swath of MISR leads to a broad gap between paths, and the discontinuity of the MISR L2 AOD data is noticeable along the swath boundary. The remaining products have similar AOD distributions in general, but with differences in magnitude that vary by region. As noted in the discussion of the land-AOD validation results using AERONET, the AHI ESR and MODIS DT give high AOD values of ~0.8 to >1.0 over eastern China (near 35°N, 120°E). The other products also show high AOD over this region, but the mean AOD of AHI MRM is ~0.8, and those of GOCI, MODIS DB, MISR, and VIIRS are 0.6–0.7. The Korean Peninsula AOD is higher in AHI MRM and ESR, and lower in MODIS DB and GOCI. Over Japan, the AOD is higher in AHI MRM, AHI ESR, and VIIRS, and lower in GOCI and MODIS DB, except for in the Hokkaido region (44°N, 135°E). The Hokkaido AOD values are higher in MODIS DT, MODIS DB, and MISR (up to 0.7), and stand in stark contrast to other regions of Japan, but those of GOCI, AHI, and VIIRS are more continuous over Japan. Manchuria (44°N–48°N, 123°E–130°E) shows higher AOD in GOCI and MODIS DB than in MODIS, AHI, and VIIRS. Because the GOCI and MODIS DB algorithms use a near-UV channel (e.g., 412 nm), for which surface reflectance is lower than for longer-wavelength visible channels, more pixels over bright surfaces (e.g., bare soil) are retrieved.

5.3 Comparison of observation frequency during the campaign

The total number of L2 AOD pixel samples within each 0.5° × 0.5° grid cell during the campaign period (Fig. 6) is labeled N_{max} and presented in Fig. 7. This number is high when the spatial and temporal resolutions are high and when fewer pixels are masked because of the presence of clouds or uncertain surface reflectance. The calculated mean AOD is more statistically representative when N_{max} is high. Highly uncertain AOD values can be removed during the spatiotemporal averaging steps, but these pixels can still lead to high uncertainty when temporally averaged mean AOD is calculated from only a few samples. Thus, we can determine the reliability of AOD values for each region and for each product using the number of L2 pixel samples. The highest N_{max} is found from AHI for which the maximum N_{max} is ~7.3×10^4; the N_{max} of GOCI peaks at 1.2×10^4. The maximum N_{max} of MODIS and MISR is 500–600 and that of VIIRS is ~1500. The higher value for VIIRS is due to its wider swath and finer L2 data resolution compared with MODIS. Similarly, the MISR has narrower swath compared to MODIS but higher spatial resolution, so it results in similar maximum N_{max} of MODIS and MISR.

Most products have more samples over the Korean Peninsula and eastern China than over Japan. Possible reason of lower sampling in Japan is higher amount of cloud due to its adjacency of the Pacific Ocean, or a combination of lower AOD condition and very high mountains and therefore slope effects, plus high spatial variance of AOD with higher values in the valleys and lower over the mountain peaks. The N_{max} of GOCI is high over the Korean Peninsula, with some discontinuity between land and ocean. The negative GOCI AOD bias under low-AOD conditions from land-surface reflectance effects results in retrieved AOD values of less than −0.05, which are screened out of the final product. This bias has less of an effect

on the land pixels of GOCI. As AHI AOD is not affected by these errors, continuously high N_{max} over land and ocean surfaces exists in the Korean Peninsula. The N_{max} of MISR includes a discontinuity between paths that results in a more discontinuous AOD distribution compared with the other products. The MODIS DT and DB have similar distributions of land N_{max}, except over Manchuria as discussed above. The MODIS DT has fewer samples over the Yellow Sea because of turbid water and sun-glint masking. The distribution of VIIRS N_{max} is similar to that of MODIS DT, but is higher over the ocean because of its broad swath thereby avoiding sun glint at times.

5.4 Daily AOD integration

Retrieved satellite AOD errors can be classified into two types: random error and bias. Although some algorithms, such as the optimal estimation method, can provide an estimated random error or uncertainty quantitatively (e.g., Jeong et al., 2016), the random error and bias of retrieved AOD can be assessed only over AERONET sites, making it difficult to quantify and validate uncertainties for all pixels. As errors were found to be distributed equally around zero for land and ocean surfaces during the validation using AERONET data, the combined AOD is calculated by selecting the median value from the daily 0.5°×0.5° gridded mean AOD. The calculated daily combined AOD is temporally averaged over the campaign period and presented in Fig. 6h. Median relative contributions for the grid and campaign period were determined for AHI ESR (33.3%), AHI MRM (31.1%), GOCI (11.3%), VIIRS (10.3%), MODIS DT (8.3%), MODIS DB (3.7%), and MISR (2.1%). Because GEO measurements yield more samples that contribute to the daily representative AOD, the AHI and GOCI account for a higher fraction of the combined AOD. For this reason, the combined AOD distribution is similar to those of AHI MRM and ESR, but the spatial distribution of the combined AOD is more continuous than that of any individual product.

Evaluation of the daily average AOD for each product and the combined AOD using daily AERONET AOD is presented in Fig. 8. The closest grid point to each AERONET site is selected for the comparison. The number of selected grid points is 870 (AHI), 768 (GOCI), 600 (VIIRS), 436 (MODIS DT), 303 (MODIS DB), and 106 (MISR). As noted in the L2 AOD validation, GOCI is negatively biased and MODIS DT is positively biased. The combined AOD has a higher f within EE_{DT} (60.9%) than the individual products, except for MISR, and a high N (869), low $RMSE$ (0.163), and high R (0.872). Thus, the combined AOD includes more pixels of high accuracy than do the individual AOD products.

6. Discussion and conclusions

In this study, we compare spatiotemporal characteristics of three GEO AOD products (GOCI, AHI MRM, and AHI ESR) and four LEO AOD products (MODIS DT, MODIS DB, MISR, and VIIRS), and validate each product using the AERONET version 3 dataset for the 2016 KORUS-AQ campaign. Most AOD products have high accuracy and wide coverage over East Asia, but each has unique characteristics (e.g. detailed accuracy and sampling frequency). Although Choi et al. (2018) showed that GOCI AOD is reliably accurate for the period 2011–2015, it is negatively biased during the 2016 campaign period. This difference in accuracy may be attributable to changes in climatological surface reflectance or calibration drift. The DT method

used in AHI ESR and MODIS DT AOD retrievals results in a positive bias and higher AOD over East Asia compared to other products. The MISR AOD has smaller coverage than MODIS and VIIRS, but the AOD accuracy is higher than for the other products because of an improved surface-reflectance treatment that takes advantage of multi-angle measurements. However, it also seems that the MISR retrievals often screen out the highest AOD events, thereby biasing the sampling in this region. These coverage and accuracy differences are due primarily to algorithm design, which is optimized for particular sensor specifications, such as the available channels, and are not due to orbit types.

As GOCI and AHI AOD can be retrieved with high accuracy at near-real-time, the highly variable AOD conditions over East Asia, including transport from Russia to Japan, transport from China to Korea, and local emissions in the SMA area and subsequent transport to the Yellow Sea, can be successfully detected. This results in more representative daily AOD values. A combined AOD using GEO and LEO data is also tested using a median-value selection at the daily scale with a 0.5° × 0.5° grid resolution. The combined AOD has a more spatially continuous distribution and higher accuracy than do the individual products. Such a combined product reduces bias in aerosol measurements and will be of use in the evaluation of air-quality models.

Although the validation using AERONET data reveal relative characteristics among the various AOD products in terms of accuracy, it is insufficient to thoroughly investigate these characteristics. Each algorithm includes subjective criteria, such as those used in cloud masking, surface-reflectance determination, aerosol model selection, inversion methods, and quality control. For example, the possible AOD range that can be retrieved and provided as the final AOD product varies among GOCI (−0.05 to 3.6), AHI (−0.05 to 3.5), MODIS DT (−1.0 to 5.0), MODIS DB (0.0 to 5.0), and MISR (0.0 to 3.0). The quality flag is also determined subjectively. This results in differences in the identification of severe pollution events (e.g., AOD > 3.0 or > 5.0) among the various products. The target regions of the GEO and LEO measurements also differ. Aerosol retrieval algorithms for LEO measurements have been developed for global coverage, but those for GEO measurements only consider the accuracy within specific regions. Because the validation datasets differ, algorithm improvement proceeds differently among the various algorithms. Thus, the integration of multiple-AOD products requires a comprehensive understanding of each product in the set. To reduce uncertainties arising from the use of different algorithms, the same algorithm can be applied to several sensors, just as the DB algorithm is applied to AVHRR, SeaWiFS, MODIS, and VIIRS measurements (Sayer et al., 2017; Lee et al., 2015; Hsu et al., 2013; Sayer et al., 2012), and the DT algorithm is applied to MODIS, VIIRS, and planned to be applied to AHI and ABI. Additionally, LEO and GEO aerosol measurements can be integrated at the resolution of radiance data as Level 1B, not retrieved AOD products, as a concept of the multi-angle measurement. This integration will enable the retrieval of other aerosol optical properties, such as particle shape or absorptivity, which can be used to evaluate aerosol optical effects along with chemical composition.

This study focuses only on the spring season of 2016 when the KORUS-AQ campaign was conducted. An extended long-term study will be required to evaluate monthly or seasonal mean AOD trends of GEO and LEO measurements and combined AOD products. Additionally, the integration of multiple datasets may be improved by a consideration of pixel-level uncertainties and varying error characteristics, pixel size, and pixel shape, and the application of more advanced statistical techniques. Other

optical properties, such as the Ångstrom exponent and single scattering albedo, should also be investigated along with AOD in future studies.

Author contributions

MC, HL, SL, JK, TE, BH, MG, EH, PS

MC and JK designed the data analysis. MC, HL, SL, JK, EH, PS carried out the GOCI and AHI data production, distribution, and analysis. MC, HL, SL, JK, TE, and BH carried out an installation, maintenance, and data analysis of the AERONET measurement during the 2016 KORUS-AQ campaign. MG provided the MISR AOD data and contributed to the data analysis. MC and JK wrote the manuscript with comments from all coauthors.

Competing interests

The authors declare that they have no conflicts of interest.

Acknowledgements

We thank all principal investigators and their staff for establishing and maintaining the AERONET sites used in this investigation. We also thank the MODIS, MISR, and VIIRS science teams for providing valuable data for this research. This research was supported by the National Strategic Project–Fine Particle of the National Research Foundation of Korea (NRF) funded by the Ministry of Science and ICT (MSIT), the Ministry of Environment (ME), and the Ministry of Health and Welfare (MOHW; NRF-2017M3D8A1092021). Some research tasks were supported by the NASA ROSES-2013 Atmospheric Composition: Aura Science Team program and NASA Headquarter Directed Research and Technology Development Task (grant number: NNN13D455T, manager: Kenneth W. Jucks and Richard S. Eckman). A portion of this research was carried out at the Jet Propulsion Laboratory, California Institute of Technology, under a contract with the National Aeronautics and Space Administration.

References

Chen, X. F., Li, Z. Q., Zhao, S. S., Yang, L. K., Ma, Y., Liu, L., Li, D. H., Qie, L. L., and Xing, J.: Using the Gaofen-4 geostationary satellite to retrieve aerosols with high spatiotemporal resolution, J Appl Remote Sens, 12, 2018.

Choi, M., Kim, J., Lee, J., Kim, M., Park, Y.-J., Holben, B., Eck, T. F., Li, Z., and Song, C. H.: GOCI Yonsei aerosol retrieval version 2 products: an improved algorithm and error analysis with uncertainty estimation from 5-year validation over East Asia, Atmos Meas Tech, 11, 385-408, 2018.

Choi, M., Kim, J., Lee, J., Kim, M., Park, Y.-J., Jeong, U., Kim, W., Hong, H., Holben, B., Eck, T. F., Song, C. H., Lim, J.-H., and Song, C.-K.: GOCI Yonsei Aerosol Retrieval (YAER) algorithm and validation during the DRAGON-NE Asia 2012 campaign, Atmos Meas Tech, 9, 1377-1398, 2016.

Cox, C. and Munk, W.: Statistics of the sea surface derived from sun glitter, Journal of Marine Research, 13, 198-227, 1954.

Daisaku, U.: Aerosol Optical Depth product derived from Himawari-8 data for Asian dust monitoring, Meteorological Satellite Center Techinical Note, 61, 2016.

Diner, D. J., Beckert, J. C., Reilly, T. H., Bruegge, C. J., Conel, J. E., Kahn, R. A., Martonchik, J. V., Ackerman, T. P., Davies, R., Gerstl, S. A. W., Gordon, H. R., Muller, J. P., Myneni, R. B., Sellers, P. J., Pinty, B., and Verstraete, M. M.: Multi-angle Imaging SpectroRadiometer (MISR) - Instrument description and experiment overview, Ieee T Geosci Remote, 36, 1072-1087, 1998.

Diner, D. J., et al.: Advances in multiangle satellite remote sensing of speciated airborne particulate matter and association with adverse health effects: from MISR to MAIA, J Appl Remote Sens, 12, 2018.

Eck, T. F., Holben, B. N., Reid, J. S., Dubovik, O., Smirnov, A., O'Neill, N. T., Slutsker, I., and Kinne, S.: Wavelength dependence of the optical depth of biomass burning, urban, and desert dust aerosols, J Geophys Res-Atmos, 104, 31333-31349, 1999.

Eck, T. F., et al.: Observations of the Interaction and Transport of Fine Mode Aerosols With Cloud and/or Fog in Northeast Asia From Aerosol Robotic Network and Satellite Remote Sensing, J Geophys Res-Atmos, 123, 5560-5587, 2018.

Garay, M. J., Kalashnikova, O. V., and Bull, M. A.: Development and assessment of a higher-spatial-resolution (4.4 km) MISR aerosol optical depth product using AERONET-DRAGON data, Atmos Chem Phys, 17, 5095-5106, 2017.

GCOS: The global observing system for climate: Implementation needs, Geneva, Switzerland, 2016.

Giles, D. M., Sinyuk, A., Sorokin, M. G., Schafer, J. S., Smirnov, A., Slutsker, I., Eck, T. F., Holben, B. N., Lewis, J. R., Campbell, J. R., Welton, E. J., Korkin, S. V., and Lyapustin, A. I.: Advancements in the Aerosol Robotic Network (AERONET) Version 3 database – automated near-real-time quality control algorithm with improved cloud screening for Sun photometer aerosol optical depth (AOD) measurements, Atmos. Meas. Tech., 12, 169-209, 2019.

Goto, D., Kikuchi, M., Suzuki, K., Hayasaki, M., Yoshida, M., Nagao, T. M., Choi, M., Kim, J., Sugimoto, N., Shimizu, A., Oikawa, E., and Nakajima, T.: Aerosol model evaluation using two geostationary satellites over East Asia in May 2016, Atmospheric Research, 217, 93-113, 2019.

Gupta, P., Levy, R. C., Mattoo, S., Remer, L. A., and Munchak, L. A.: A surface reflectance scheme for retrieving aerosol optical depth over urban surfaces in MODIS Dark Target retrieval algorithm, Atmos Meas Tech, 9, 3293-3308, 2016.

Herman, J. R. and Celarier, E. A.: Earth surface reflectivity climatology at 340-380 nm from TOMS data, J Geophys Res-Atmos, 102, 28003-28011, 1997.

Higurashi, A. and Nakajima, T.: Development of a two-channel aerosol retrieval algorithm on a global scale using NOAA AVHRR, J Atmos Sci, 56, 924-941, 1999.

Holben, B. N., Eck, T. F., Slutsker, I., Tanre, D., Buis, J. P., Setzer, A., Vermote, E., Reagan, J. A., Kaufman, Y. J., Nakajima, T., Lavenu, F., Jankowiak, I., and Smirnov, A.: AERONET - A federated instrument network and data archive for aerosol characterization, Remote Sens Environ, 66, 1-16, 1998.

Holben, B. N., et al.: An overview of mesoscale aerosol processes, comparisons, and validation studies from DRAGON networks, Atmos Chem Phys, 18, 655-671, 2018.

Hsu, N. C., Jeong, M. J., Bettenhausen, C., Sayer, A. M., Hansell, R., Seftor, C. S., Huang, J., and Tsay, S. C.: Enhanced Deep Blue aerosol retrieval algorithm: The second generation, J Geophys Res-Atmos, 118, 9296-9315, 2013.

Hsu, N. C., Tsay, S. C., King, M. D., and Herman, J. R.: Aerosol properties over bright-reflecting source regions, Ieee T Geosci Remote, 42, 557-569, 2004.

Huang, J. F., Kondragunta, S., Laszlo, I., Liu, H. Q., Remer, L. A., Zhang, H., Superczynski, S., Ciren, P., Holben, B. N., and Petrenko, M.: Validation and expected error estimation of Suomi-NPP VIIRS aerosol optical thickness and Angstrom exponent with AERONET, J Geophys Res-Atmos, 121, 7139-7160, 2016.

Hyer, E. J., Reid, J. S., and Zhang, J.: An over-land aerosol optical depth data set for data assimilation by filtering, correction, and aggregation of MODIS Collection 5 optical depth retrievals, Atmos Meas Tech, 4, 379-408, 2011.

IPCC: Climate Change 2013: The Physical Science Basis. Contribution of Working Group I to the Fifth Assessment Report of the Intergovernmental Panel on Climate Change, Cambridge University Press, Cambridge, United Kingdom and New York, NY, USA, 2013.

Jackson, J. M., Liu, H. Q., Laszlo, I., Kondragunta, S., Remer, L. A., Huang, J. F., and Huang, H. C.: Suomi-NPP VIIRS aerosol algorithms and data products, J Geophys Res-Atmos, 118, 12673-12689, 2013.

Jacob, D. J., Crawford, J. H., Kleb, M. M., Connors, V. S., Bendura, R. J., Raper, J. L., Sachse, G. W., Gille, J. C., Emmons, L., and Heald, C. L.: Transport and Chemical Evolution over the Pacific (TRACE-P) aircraft mission: Design, execution, and first results, Journal of Geophysical Research: Atmospheres, 108, 2003.

Jeon, W., Choi, Y., Percell, P., Souri, A. H., Song, C. K., Kim, S. T., and Kim, J.: Computationally efficient air quality forecasting tool: implementation of STOPS v1.5 model into CMAQ v5.0.2 for a prediction of Asian dust, Geosci Model Dev, 9, 3671-3684, 2016.

Jeong, U., Kim, J., Ahn, C., Torres, O., Liu, X., Bhartia, P. K., Spurr, R. J. D., Haffner, D., Chance, K., and Holben, B. N.: An optimal-estimation-based aerosol retrieval algorithm using OMI near-UV observations, Atmos Chem Phys, 16, 177-193, 2016.

Kaufman, Y. J., Tanre, D., Remer, L. A., Vermote, E. F., Chu, A., and Holben, B. N.: Operational remote sensing of tropospheric aerosol over land from EOS moderate resolution imaging spectroradiometer, J Geophys Res-Atmos, 102, 17051-17067, 1997.

Kikuchi, M., Murakami, H., Suzuki, K., Nagao, T. M., and Higurashi, A.: Improved Hourly Estimates of Aerosol Optical Thickness Using Spatiotemporal Variability Derived From Himawari-8 Geostationary Satellite, Ieee T Geosci Remote, 56, 3442-3455, 2018.

Kim, J., Yoon, J. M., Ahn, M. H., Sohn, B. J., and Lim, H. S.: Retrieving aerosol optical depth using visible and mid-IR channels from geostationary satellite MTSAT-1R, Int J Remote Sens, 29, 6181-6192, 2008.

Kim, M., Kim, J., Jeong, U., Kim, W., Hong, H., Holben, B., Eck, T. F., Lim, J. H., Song, C. K., Lee, S., and Chung, C. Y.: Aerosol optical properties derived from the DRAGON-NE Asia campaign, and implications for a single-channel algorithm to retrieve aerosol optical depth in spring from Meteorological Imager (MI) on-board the Communication, Ocean, and Meteorological Satellite (COMS), Atmos Chem Phys, 16, 1789-1808, 2016.

Kim, S. W., Yoon, S. C., Kim, J., and Kim, S. Y.: Seasonal and monthly variations of columnar aerosol optical properties over east Asia determined from multi-year MODIS, LIDAR, and AERONET Sun/sky radiometer measurements, Atmos Environ, 41, 1634-1651, 2007.

Kim, Y. P., Lee, G., Emmons, L., Park, R., and Lin, N. H.: Preface to a Special Issue "Megacity Air Pollution Studies (MAPS)", Aerosol and Air Quality Research, 18, I-Iv, 2018.

Knapp, K. R., Vonder Haar, T. H., and Kaufman, Y. J.: Aerosol optical depth retrieval from GOES-8: Uncertainty study and retrieval validation over South America, J Geophys Res-Atmos, 107, 4055, doi:4010.1029/2001JD000505, 2002.

Koelemeijer, R. B. A., de Haan, J. F., and Stammes, P.: A database of spectral surface reflectivity in the range 335-772 nm derived from 5.5 years of GOME observations, J Geophys Res-Atmos, 108, 4070, doi:4010.1029/2002jd002429, 2003.

Laszlo, I. and Liu, H.: EPS Aerosol Optical Depth (AOD) Algorithm Theoretical Basis Document, NOAA NESDIS Center for Satellite Applications and Research, 2016. 2016.

Lee, J., Hsu, N. C., Bettenhausen, C., Sayer, A. M., Seftor, C. J., and Jeong, M. J.: Retrieving the height of smoke and dust aerosols by synergistic use of VIIRS, OMPS, and CALIOP observations, J Geophys Res-Atmos, 120, 8372-8388, 2015.

Lee, J., Kim, J., Song, C. H., Ryu, J. H., Ahn, Y. H., and Song, C. K.: Algorithm for retrieval of aerosol optical properties over the ocean from the Geostationary Ocean Color Imager, Remote Sens Environ, 114, 1077-1088, 2010.

Lee, S., Hong, J., Cho, Y., Choi, M., Kim, J., Park, S. S., Ahn, J. Y., Kim, S. K., Moon, K. J., Eck, T. F., Holben, B. N., and Koo, J. H.: Characteristics of Classified Aerosol Types in South Korea during the MAPS-Seoul Campaign, Aerosol and Air Quality Research, 18, 2195-2206, 2018.

Lee, S., Song, C. H., Park, R. S., Park, M. E., Han, K. M., Kim, J., Choi, M., Ghim, Y. S., and Woo, J. H.: GIST-PM-Asia v1: development of a numerical system to improve particulate matter forecasts in South Korea using geostationary satellite-retrieved aerosol optical data over Northeast Asia, Geosci Model Dev, 9, 17-39, 2016.

Lennartson, E. M., Wang, J., Gu, J., Castro Garcia, L., Ge, C., Gao, M., Choi, M., Saide, P. E., Carmichael, G. R., Kim, J., and Janz, S. J.: Diurnal variation of aerosol optical depth and PM2.5 in South Korea: a synthesis from AERONET, satellite (GOCI), KORUS-AQ observation, and the WRF-Chem model, Atmos. Chem. Phys., 18, 15125-15144, 2018.

Levy, R. C., Mattoo, S., Munchak, L. A., Remer, L. A., Sayer, A. M., Patadia, F., and Hsu, N. C.: The Collection 6 MODIS aerosol products over land and ocean, Atmos Meas Tech, 6, 2989-3034, 2013.

Levy, R. C., Mattoo, S., Sawyer, V., Shi, Y. X., Colarco, P. R., Lyapustin, A. I., Wang, Y. J., and Remer, L. A.: Exploring systematic offsets between aerosol products from the two MODIS sensors, Atmos Meas Tech, 11, 4073-4092, 2018.

Levy, R. C., Remer, L. A., Mattoo, S., Vermote, E. F., and Kaufman, Y. J.: Second-generation operational algorithm: Retrieval of aerosol properties over land from inversion of Moderate Resolution Imaging Spectroradiometer spectral reflectance, J Geophys Res-Atmos, 112, D13211, doi:13210.11029/12006jd007811, 2007.

Lim, H., Choi, M., Kim, J., Kasai, Y., and Chan, P.: AHI/Himawari-8 Yonsei Aerosol Retrieval (YAER): Algorithm, Validation and Merged Products, Remote Sens-Basel, 10, 699, 2018.

Lim, S. S., et al.: A comparative risk assessment of burden of disease and injury attributable to 67 risk factors and risk factor clusters in 21 regions, 1990-2010: a systematic analysis for the Global Burden of Disease Study 2010, Lancet, 380, 2224-2260, 2012.

Munchak, L. A., Levy, R. C., Mattoo, S., Remer, L. A., Holben, B. N., Schafer, J. S., Hostetler, C. A., and Ferrare, R. A.: MODIS 3 km aerosol product: applications over land in an urban/suburban region, Atmos Meas Tech, 6, 1747-1759, 2013.

Nakajima, T., Yoon, S. C., Ramanathan, V., Shi, G. Y., Takemura, T., Higurashi, A., Takamura, T., Aoki, K., Sohn, B. J., Kim, S. W., Tsuruta, H., Sugimoto, N., Shimizu, A., Tanimoto, H., Sawa, Y., Lin, N. H., Lee, C. T., Goto, D., and Schutgens, N.: Overview of the Atmospheric Brown Cloud East Asian Regional Experiment 2005 and a study of the aerosol direct radiative forcing in east Asia, J Geophys Res-Atmos, 112, 2007.

Pang, J. M., Liu, Z. Q., Wang, X. M., Bresch, J., Ban, J. M., Cnen, D., and Kim, J.: Assimilating AOD retrievals from GOCI and VIIRS to forecast surface PM2.5 episodes over Eastern China, Atmos Environ, 179, 288-304, 2018.

Park, M. E., Song, C. H., Park, R. S., Lee, J., Kim, J., Lee, S., Woo, J. H., Carmichael, G. R., Eck, T. F., Holben, B. N., Lee, S. S., Song, C. K., and Hong, Y. D.: New approach to monitor transboundary particulate pollution over Northeast Asia, Atmos Chem Phys, 14, 659-674, 2014.

Park, S., Shin, M., Im, J., Song, C. K., Choi, M., Kim, J., Lee, S., Park, R., Kim, J., Lee, D. W., and Kim, S. K.: Estimation of ground level particulate matter concentrations through the synergistic use of satellite observations and process-based models over South Korea, Atmos. Chem. Phys. Discuss., 2018, 1-26, 2018.

Remer, L. A., Kaufman, Y. J., Tanré, D., Mattoo, S., Chu, D. A., Martins, J. V., Li, R. R., Ichoku, C., Levy, R. C., Kleidman, R. G., Eck, T. F., Vermote, E., and Holben, B. N.: The MODIS Aerosol Algorithm, Products, and Validation, J Atmos Sci, 62, 947-973, 2005.

Saide, P. E., Kim, J., Song, C. H., Choi, M., Cheng, Y. F., and Carmichael, G. R.: Assimilation of next generation geostationary aerosol optical depth retrievals to improve air quality simulations, Geophys Res Lett, 41, 9188-9196, 2014.

Sayer, A. M., Hsu, N. C., Bettenhausen, C., Ahmad, Z., Holben, B. N., Smirnov, A., Thomas, G. E., and Zhang, J.: SeaWiFS Ocean Aerosol Retrieval (SOAR): Algorithm, validation, and comparison with other data sets, J Geophys Res-Atmos, 117, D03206, doi:03210.01029/02011jd016599, 2012.

Sayer, A. M., Hsu, N. C., Bettenhausen, C., and Jeong, M. J.: Validation and uncertainty estimates for MODIS Collection 6 "Deep Blue" aerosol data, J Geophys Res-Atmos, 118, 7864-7872, 2013.

Sayer, A. M., Hsu, N. C., Lee, J., Carletta, N., Chen, S.-H., and Smirnov, A.: Evaluation of NASA Deep Blue/SOAR aerosol retrieval algorithms applied to AVHRR measurements, Journal of Geophysical Research: Atmospheres, 122, 9945-9967, 2017.

Sayer, A. M., Munchak, L. A., Hsu, N. C., Levy, R. C., Bettenhausen, C., and Jeong, M. J.: MODIS Collection 6 aerosol products: Comparison between Aqua's e-Deep Blue, Dark Target, and "merged" data sets, and usage recommendations, J Geophys Res-Atmos, 119, 13965-13989, 2014.

Torres, O., Bhartia, P. K., Herman, J. R., Ahmad, Z., and Gleason, J.: Derivation of aerosol properties from satellite measurements of backscattered ultraviolet radiation: Theoretical basis, J Geophys Res-Atmos, 103, 17099-17110, 1998.

Urm, Y.-D. and Sohn, B.-J.: Estimation of aerosol optical thickness over east asia using GMS-5 visible channel measurements, Journal of Atmosphere, 15, 203-211, 2005.

Wang, J., Christopher, S. A., Brechtel, F., Kim, J., Schmid, B., Redemann, J., Russell, P. B., Quinn, P., and Holben, B. N.: Geostationary satellite retrievals of aerosol optical thickness during ACE-Asia, J Geophys Res-Atmos, 108, 8657, doi:8610.1029/2003jd003580, 2003.

Witek, M. L., Garay, M. J., Diner, D. J., Bull, M. A., and Seidel, F. C.: New approach to the retrieval of AOD and its uncertainty from MISR observations over dark water, Atmos Meas Tech, 11, 429-439, 2018.

Xiao, Q., Zhang, H., Choi, M., Li, S., Kondragunta, S., Kim, J., Holben, B., Levy, R. C., and Liu, Y.: Evaluation of VIIRS, GOCI, and MODIS Collection 6AOD retrievals against ground sunphotometer observations over East Asia, Atmos Chem Phys, 16, 1255-1269, 2016.

Yoon, J., Burrows, J. P., Vountas, M., von Hoyningen-Huene, W., Chang, D. Y., Richter, A., and Hilboll, A.: Changes in atmospheric aerosol loading retrieved from space-based measurements during the past decade, Atmos Chem Phys, 14, 6881-6902, 2014.

Yoon, J. M., Kim, J., Lee, J. H., Cho, H. K., Sohn, B. J., and Ahn, M. H.: Retrieval of Aerosol Optical Depth over East Asia from a Geostationary Satellite, MTSAT-1R, Asia-Pac J Atmos Sci, 43, 133-142, 2007.

Zhang, J. L. and Reid, J. S.: MODIS aerosol product analysis for data assimilation: Assessment of over-ocean level 2 aerosol optical thickness retrievals, J Geophys Res-Atmos, 111, 2006.

Zhang, W. H., Xu, H., and Zheng, F. J.: Aerosol Optical Depth Retrieval over East Asia Using Himawari-8/AHI Data, Remote Sens-Basel, 10, 2018.

Atmos. Meas. Tech. Discuss., https://doi.org/10.5194/amt-2019-46
Manuscript under review for journal Atmos. Meas. Tech.
Discussion started: 18 March 2019

Atmospheric Measurement Techniques Discussions

Tables

Table 1 Characteristics of multi-sensor aerosol products.

Sensor / Platform (orbit type)	GOCI / COMS (GEO)	AHI / Himawari-8 (GEO)	MODIS / Terra, Aqua (LEO)	VIIRS / Suomi-NPP (LEO)	MISR / Terra (LEO)
Swath for LEO or local coverage for GEO	2500 km × 2500 km area over East Asia centered at 130°E, 36°N	Full disk centered at 140.7°E	2330 km	3040 km	380 km
Algorithm version	Yonsei Aerosol Retrieval version 2	Yonsei Aerosol Retrieval	Dark-Target Collection 6.1; Deep-Blue Collection 6.1 (land-only)	Environmental Data Records	Version 23
Measurement time (Local Standard Time over Korea)	1 h interval from 09:30 to 16:30 (totally 8 times during daylight)	10 min interval for full-disk measurements (only 09:00–16:50 in this study)	10:30 for Terra 13:30 for Aqua	13:25	10:30
Spatial resolution of aerosol products (nadir point for LEO)	6 km × 6 km	6 km × 6 km	10 km × 10 km and 3 km × 3 km for DT, 10 km × 10 km for DB	6 km × 6 km for EDR	4.4 km × 4.4 km
References	Choi et al. (2018); Choi et al. (2016)	Lim et al. (2018)	Gupta et al. (2016); Levy et al. (2018)	Huang et al. (2016); Jackson et al. (2013)	Garay et al. (2017); Witek et al. (2018)

Atmos. Meas. Tech. Discuss., https://doi.org/10.5194/amt-2019-46
Manuscript under review for journal Atmos. Meas. Tech.
Discussion started: 18 March 2019

Atmospheric Measurement Techniques Discussions

Table 2 Validation statistics for land AOD products.

Land AOD	*N*	*R*	*RMSE*	*Mean bias*	*f* within EE_{DT}
GOCI 6 km (10:30 LST)	551	0.927	0.135	−0.060	0.515
GOCI 6 km (13:30 LST)	559	0.894	0.141	−0.054	0.479
GOCI 6 km (all 8 hourly meas.)	**4292**	**0.906**	**0.151**	**−0.072**	**0.477**
AHI MRM 6 km (10:30 LST)	607	0.886	0.157	−0.031	0.600
AHI MRM 6 km (13:30 LST)	636	0.900	0.136	−0.019	0.608
AHI MRM 6 km (every 90 min)	4,826	0.887	0.157	−0.045	0.580
AHI MRM 6 km (all 10 min interval meas.)	**19160**	**0.910**	**0.144**	**−0.061**	**0.584**
AHI ESR 6 km (10:30 LST)	608	0.894	0.180	0.104	0.487
AHI ESR 6 km (13:30 LST)	637	0.904	0.184	0.128	0.405
AHI ESR 6 km (every 90 min)	4,830	0.888	0.172	0.084	0.507
AHI ESR 6 km (all 10 min interval meas.)	**19174**	**0.901**	**0.155**	**0.074**	**0.537**
MODIS DT 10 km (Terra)	501	0.874	0.245	0.128	0.491
MODIS DT 10 km (Aqua)	487	0.856	0.186	0.099	0.538
MODIS DT 10 km (Terra and Aqua)	**988**	**0.868**	**0.218**	**0.113**	**0.514**
MODIS DT 3 km (Terra)	651	0.877	0.221	0.140	0.444
MODIS DT 3 km (Aqua)	661	0.886	0.246	0.161	0.418
MODIS DT 3 km (Terra and Aqua)	**1312**	**0.882**	**0.234**	**0.150**	**0.431**
MODIS DB 10 km (Terra)	438	0.892	0.175	0.067	0.521
MODIS DB 10 km (Aqua)	413	0.870	0.165	0.068	0.538
MODIS DB 10 km (Terra and Aqua)	**851**	**0.883**	**0.170**	**0.068**	**0.529**
MISR 4.4 km (Terra)	**114**	**0.933**	**0.118**	**−0.023**	**0.807**
VIIRS EDR 6 km (Suomi-NPP)	**800**	**0.872**	**0.157**	**0.066**	**0.588**

Atmos. Meas. Tech. Discuss., https://doi.org/10.5194/amt-2019-46
Manuscript under review for journal Atmos. Meas. Tech.
Discussion started: 18 March 2019

Atmospheric Measurement Techniques Discussions

Table 3 As for Table 2, except for ocean AOD products.

Ocean AOD	*N*	*R*	*RMSE*	*Mean Bias*	*f* within EE_{DT}
GOCI 6 km (10:30 LST)	221	0.909	0.109	0.037	0.742
GOCI 6 km (13:30 LST)	230	0.871	0.140	0.056	0.648
GOCI 6 km (all 8 hourly meas.)	**1766**	**0.884**	**0.118**	**0.026**	**0.677**
AHI MRM 6 km (10:30 LST)	232	0.878	0.122	−0.020	0.616
AHI MRM 6 km (13:30 LST)	241	0.864	0.138	−0.004	0.581
AHI MRM 6 km (every 90 min)	1849	0.871	0.131	−0.021	0.613
AHI MRM 6 km (all 10 min interval meas.)	**7575**	**0.870**	**0.126**	**−0.034**	**0.643**
AHI ESR 6 km (10:30 LST)	234	0.894	0.111	0.046	0.688
AHI ESR 6 km (13:30 LST)	247	0.805	0.153	0.052	0.656
AHI ESR 6 km (every 90 min)	1879	0.848	0.131	0.030	0.715
AHI ESR 6 km (all 10 min interval meas.)	**7663**	**0.835**	**0.128**	**0.024**	**0.757**
MODIS DT 10 km (Terra)	40	0.921	0.141	0.101	0.475
MODIS DT 10 km (Aqua)	45	0.921	0.094	0.031	0.733
MODIS DT 10 km (Terra and Aqua)	**85**	**0.911**	**0.119**	**0.064**	**0.612**
MODIS DT 3 km (Terra)	94	0.916	0.168	0.119	0.372
MODIS DT 3 km (Aqua)	111	0.798	0.156	0.081	0.595
MODIS DT 3 km (Terra and Aqua)	**205**	**0.868**	**0.162**	**0.098**	**0.493**
MISR 4.4 km (Terra)	**13**	**0.626**	**0.154**	**0.035**	**0.769**
VIIRS EDR 6 km (Suomi-NPP)	**252**	**0.840**	**0.117**	**0.037**	**0.690**

Atmos. Meas. Tech. Discuss., https://doi.org/10.5194/amt-2019-46
Manuscript under review for journal Atmos. Meas. Tech.
Discussion started: 18 March 2019

Atmospheric Measurement Techniques Discussions

Figures

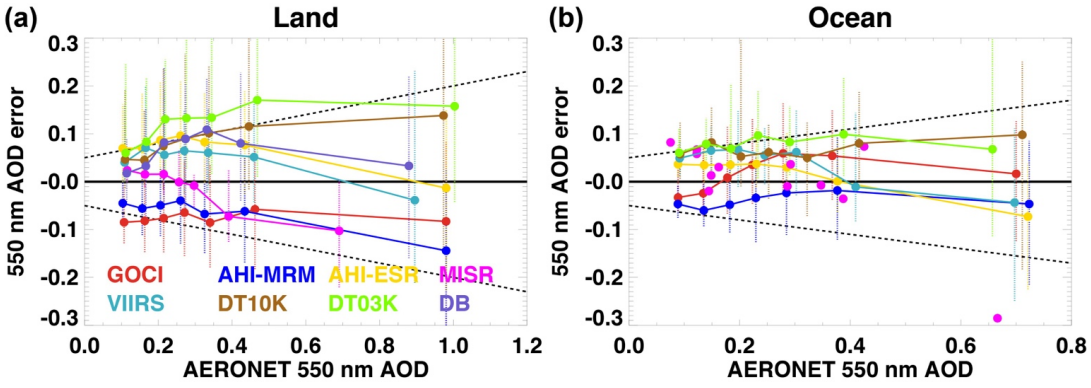

Figure 1. Comparison of observed (a) land and (b) ocean AOD errors for AERONET AOD. For each product, the total collocated data are grouped into 7 bins according to AERONET AOD, except for MISR ocean AOD errors because of low collocation numbers. Each symbol and vertical line indicate the median error and the 16th–84th percentile range for each collocated point, respectively. Black lines indicate zero difference and the EE_{DT} range $\pm(0.05 + 0.15 \times AOD_{AERONET})$.

Atmos. Meas. Tech. Discuss., https://doi.org/10.5194/amt-2019-46
Manuscript under review for journal Atmos. Meas. Tech.
Discussion started: 18 March 2019

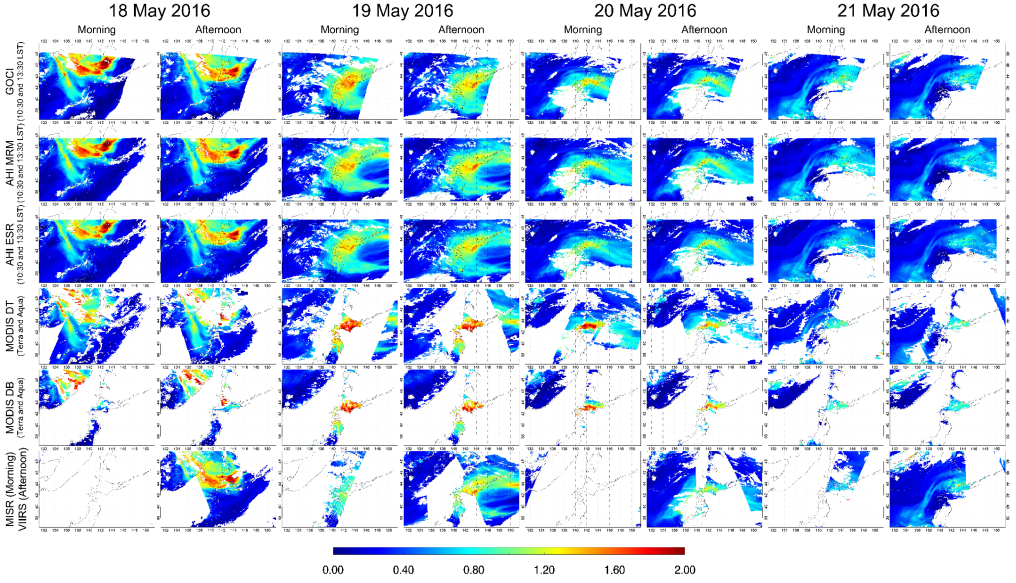

Figure 2. AOD distributions from GOCI, AHI MRM, AHI ESR, MODIS DT10K, MODIS DB, MISR, and VIIRS over the Hokkaido region during 18–21 May 2016. Note that morning and afternoon AODs for GOCI and AHI refer to 10:30 and 13:30 LST, respectively, and for MODIS these refer to the Terra and Aqua measurements, respectively. MISR has only a morning measurement and VIIRS has only an afternoon measurement.

Atmos. Meas. Tech. Discuss., https://doi.org/10.5194/amt-2019-46
Manuscript under review for journal Atmos. Meas. Tech.
Discussion started: 18 March 2019

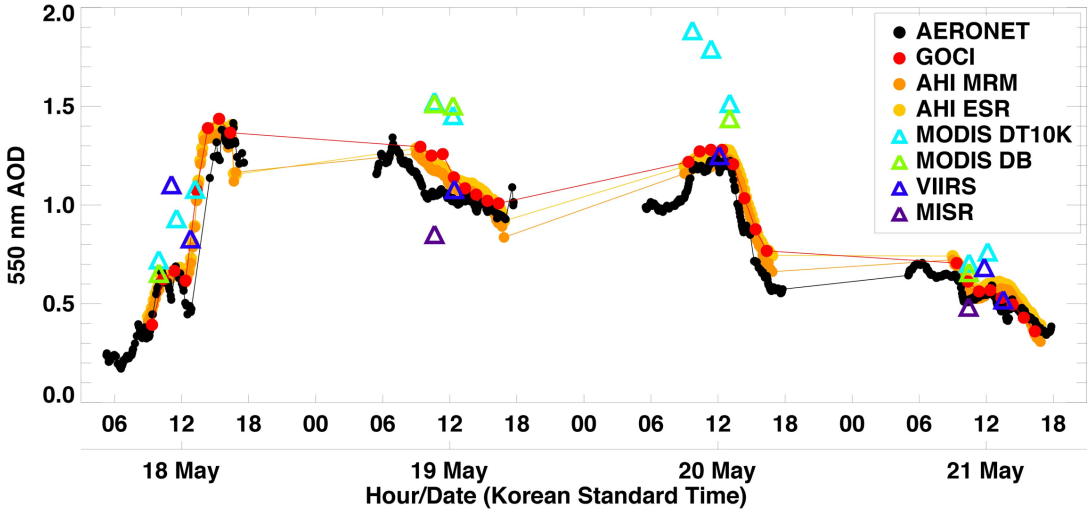

Figure 3. Time series of multiple satellite AODs and AERONET AOD at the Hokkaido University site during 18–21 May 2016.

Atmos. Meas. Tech. Discuss., https://doi.org/10.5194/amt-2019-46
Manuscript under review for journal Atmos. Meas. Tech.
Discussion started: 18 March 2019

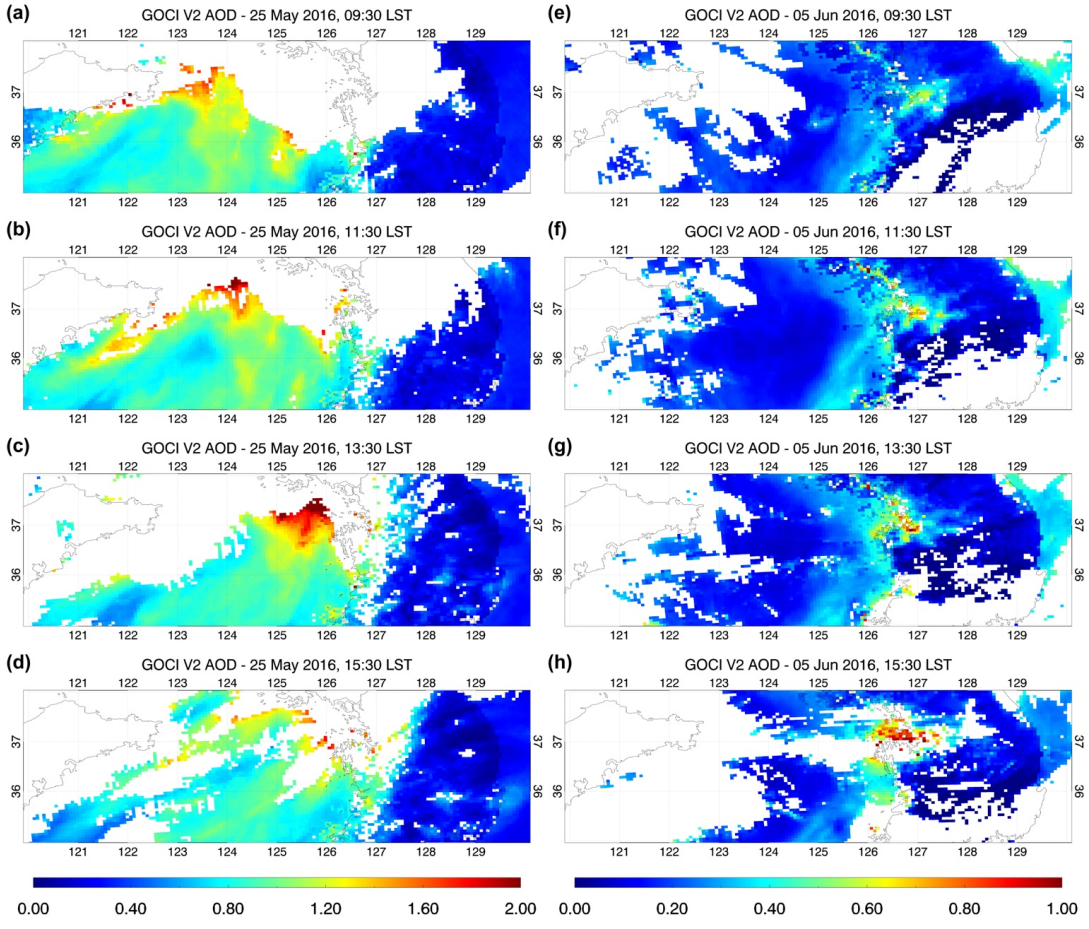

Figure 4. GOCI AOD over the Yellow Sea and Korean Peninsula (122°E–130°E and 35°N–38°N) at (a) 09:30, (b) 11:30, (c) 13:30, and (d) 15:30 LST on 25 May; (e)–(h) as for (a)–(d), but for 5 June 2016. Note that the AOD color scale is 0.0−2.0 and 0.0-1.0 for (a)−(d) and (e)−(h), respectively.

Atmos. Meas. Tech. Discuss., https://doi.org/10.5194/amt-2019-46
Manuscript under review for journal Atmos. Meas. Tech.
Discussion started: 18 March 2019

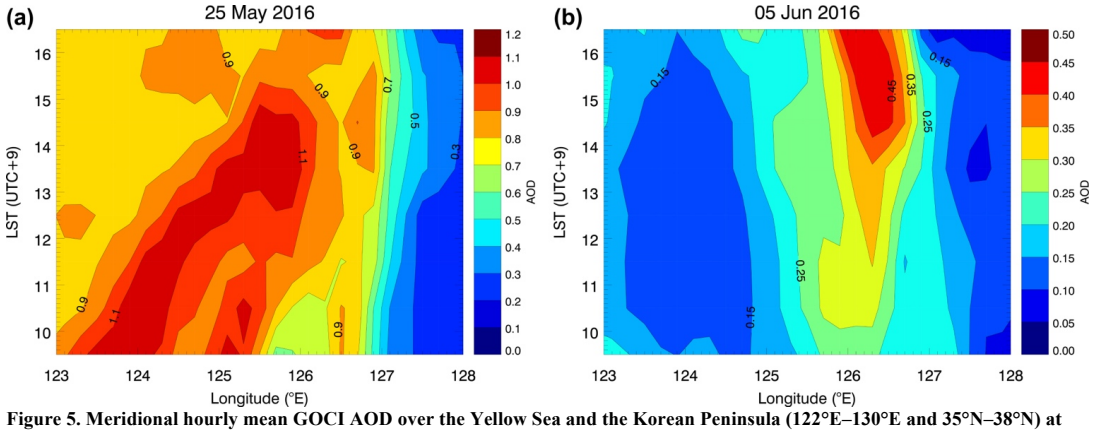

Figure 5. Meridional hourly mean GOCI AOD over the Yellow Sea and the Korean Peninsula (122°E–130°E and 35°N–38°N) at 0.2° longitude intervals on (a) 25 May and (b) 5 June 2016.

Atmos. Meas. Tech. Discuss., https://doi.org/10.5194/amt-2019-46
Manuscript under review for journal Atmos. Meas. Tech.
Discussion started: 18 March 2019

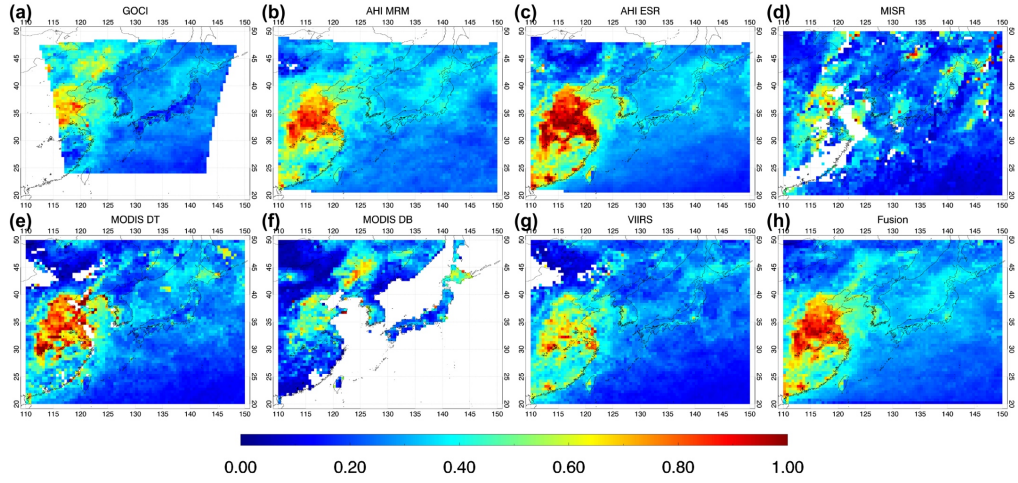

Figure 6. Mean AOD of the (a) GOCI, (b) AHI MRM, (c) AHI ESR, (d) MISR, (e) MODIS DT10K, (f) MODIS DB, (g) VIIRS, and (h) fusion products during the KORUS-AQ campaign period (1 May to 12 June 2016). The daily AOD from each product is averaged within each grid cell (0.5° × 0.5° longitude–latitude).

Atmos. Meas. Tech. Discuss., https://doi.org/10.5194/amt-2019-46
Manuscript under review for journal Atmos. Meas. Tech.
Discussion started: 18 March 2019

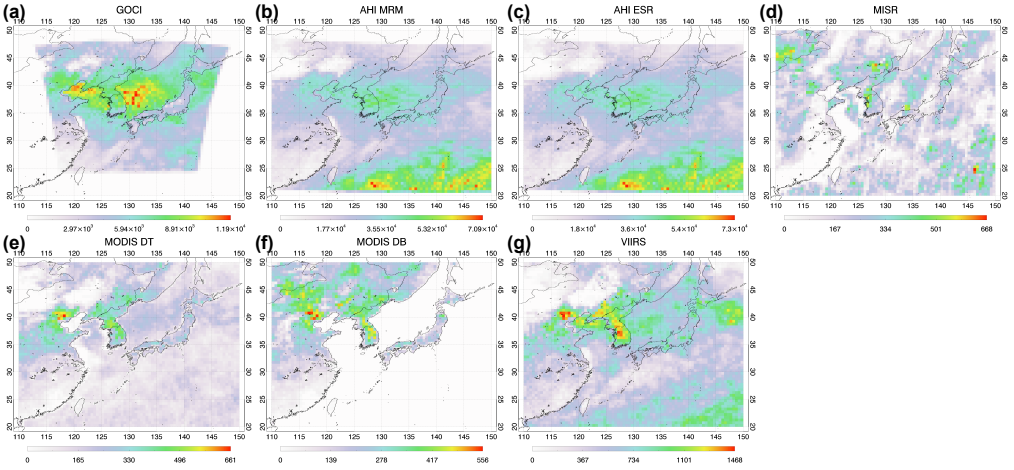

Figure 7. Number of L2 AOD pixels used to calculate the mean AOD (shown in Fig. 6) during the campaign within each 0.5° × 0.5° grid cell. Panels (a) to (g) are for the GOCI, AHI MRM, AHI ESR, MISR, MODIS DT, MODIS DB, and VIIRS products, respectively. Note that the color-scale is different for all panels.

Atmos. Meas. Tech. Discuss., https://doi.org/10.5194/amt-2019-46
Manuscript under review for journal Atmos. Meas. Tech.
Discussion started: 18 March 2019

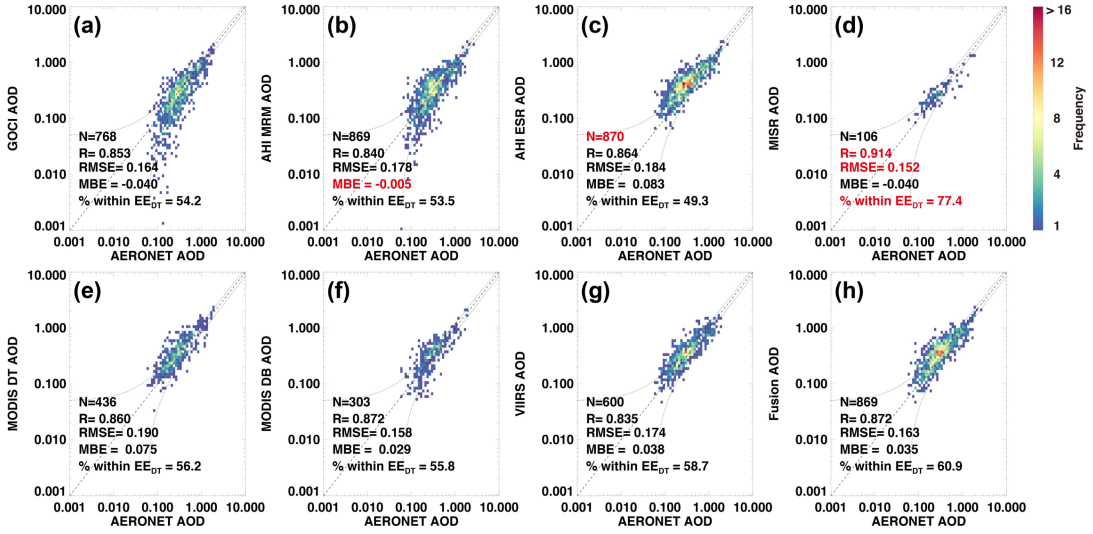

Figure 8. Validation of daily-mean AOD using AERONET daily mean AOD during the KORUS-AQ campaign period (1 May to 12 June 2016) for the (a) GOCI, (b) AHI MRM, (c) AHI ESR, (d) MISR, (e) MODIS DT10K, (f) MODIS DB, (g) VIIRS, and (h) fusion products. Lines indicate the one-to-one line (dashed) and the range of EE_{DT} (dotted). Note that the best value of each statistical metric among seven individual products (except the fusion product) are highlighted in red color.